Title

Coordinated increase of reliable cortical and striatal ensemble activations during recovery after stroke

Journal

Cell Reports, 36(2)

ISSN

2639-1856

Authors

Guo, Ling
Kondapavulur, Sravani
Lemke, Stefan M
et al.

Publication Date

2021-07-01

DOI

10.1016/j.celrep.2021.109370

Peer reviewed

HHS Public Access

Author manuscript

Cell Rep. Author manuscript; available in PMC 2021 August 11.

Published in final edited form as:

Cell Rep. 2021 July 13; 36(2): 109370. doi:10.1016/j.celrep.2021.109370.

Coordinated increase of reliable cortical and striatal ensemble activations during recovery after stroke

Ling Guo[1,2,3], **Sravani Kondapavulur**[2,3,4,5], **Stefan M. Lemke**[1,2,3], **Seok Joon Won**[2,3], **Karunesh Ganguly**[2,3,5,6,7,*]

[1]Neuroscience Graduate Program, University of California, San Francisco, San Francisco, CA 94158, USA

[2]Neurology and Rehabilitation Service, San Francisco Veterans Affairs Medical Center, San Francisco, CA 94121, USA

[3]Department of Neurology & Weill Institute for Neuroscience, University of California, San Francisco, San Francisco, CA 94158, USA

[4]Medical Scientist Training Program, University of California, San Francisco, San Francisco, CA 94158, USA

[5]Bioengineering Graduate Program, University of California, San Francisco, San Francisco, CA 94158, USA

[6]Kavli Institute for Fundamental Neuroscience, University of California, San Francisco, San Francisco, CA 94158, USA

[7]Lead contact

SUMMARY

Skilled movements rely on a coordinated cortical and subcortical network, but how this network supports motor recovery after stroke is unknown. Previous studies focused on the perilesional cortex (PLC), but precisely how connected subcortical areas reorganize and coordinate with PLC is unclear. The dorsolateral striatum (DLS) is of interest because it receives monosynaptic inputs from motor cortex and is important for learning and generation of fast reliable actions. Using a rat focal stroke model, we perform chronic electrophysiological recordings in motor PLC and DLS during long-term recovery of a dexterous skill. We find that recovery is associated with the simultaneous emergence of reliable movement-related single-trial ensemble spiking in both structures along with increased cross-area alignment of spiking. Our study highlights the

*Correspondence: karunesh.ganguly@ucsf.edu.

AUTHOR CONTRIBUTIONS

L.G. and K.G. conceived and designed the experiments. L.G. conducted the experiments and analyzed the data. S.K. assisted with the infusion experiments. S.M.L. performed striatal recordings in intact animals. S.-J.W. performed the stroke induction and conducted the histological analysis. L.G. and K.G. wrote and edited the manuscript. All authors read and edited the manuscript.

DECLARATION OF INTERESTS

The authors declare no competing interests.

SUPPLEMENTAL INFORMATION

Supplemental information can be found online at https://doi.org/10.1016/j.celrep.2021.109370.

importance of consistent neural activity patterns across brain structures during recovery and suggests that modulation of cross-area coordination can be a therapeutic target for enhancing motor function post-stroke.

In brief

Guo et al. find that recovery of movement control after motor cortical stroke is associated with reliable neural activation and coordinated activity in both perilesional cortex (PLC) and dorsolateral striatum (DLS). Neural organization occurs simultaneously in PLC and DLS. Their results highlight the importance of distributed network changes after stroke.

Graphical Abstract

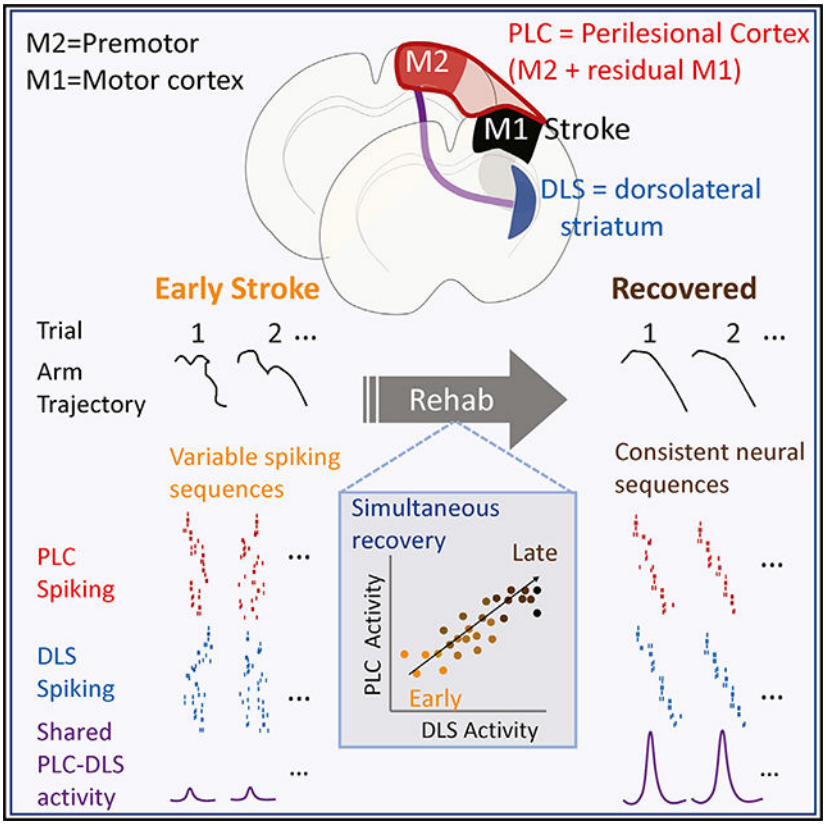

INTRODUCTION

The time-varying activations of neural ensembles represent the neural computations underlying complex behaviors (Buzsáki, 2010; Vyas et al., 2020). For skilled movement control, coordinated ensembles both local to primary motor cortex (M1) and distributed across a cortical and subcortical motor network are essential for the learning and execution of motor skills (Whishaw et al., 1986; Houk and Wise, 1995; Costa, Cohen and Nicolelis, 2004; Doyon and Benali, 2005; Yin et al., 2009; Lemke et al., 2019; Wagner et al., 2019; Sauerbrei et al., 2020). Understanding how local and cross-area ensemble dynamics change after stroke and with rehabilitation can provide important insights into how the

motor network supports recovery and for developing targeted neuromodulation methods (Ganguly et al., 2013; Liu et al., 2018; Ramanathan et al., 2018; Khanna et al., 2021). While recent studies have found evidence for the reemergence of coordinated population dynamics in perilesional cortex (PLC) after a focal M1 stroke (Ramanathan et al., 2018; Latifi et al., 2020; Khanna et al., 2021), it remains unclear how ensembles in downstream subcortical motor areas change after stroke and with recovery. Notably, past neuroimaging and anatomical studies indicate that both cortical and subcortical areas are affected by acquired brain injuries such as stroke (Chollet et al., 1991; Grefkes and Ward, 2014; Corbetta et al., 2015); connected motor areas that receive inputs from the stroke site can also be affected (known as diaschisis; von Monakow, 1914; Carrera and Tononi, 2014) and even atrophy over time (Baudat et al., 2020). Neuroimaging studies in human stroke patients provide evidence for changes in functional connectivity across cortical motor areas (Chollet et al., 1991; Ward et al., 2003; Cramer, 2008; Grefkes and Ward, 2014) and between cortical and subcortical targets (Rüber et al., 2012). Despite this knowledge about the importance of subcortical regions and the growing understanding of the spatial mapping of cortical projections to subcortical regions (Costa et al., 2004; Hintiryan et al., 2016; Peters et al., 2019), it is unknown how movement-related neural ensembles in subcortical networks change after stroke and with recovery and whether this occurs in a coordinated manner with cortical regions.

This study focused on how ensemble spiking dynamics in the dorsolateral striatum (DLS) is affected in a commonly used experimental model of a focal M1 stroke (Corbett et al., 2017) and how they change with recovery, especially in comparison to PLC, i.e., premotor cortex (M2) and areas anterior to the M1 stroke site. DLS is an important subcortical motor area that receives extensive monosynaptic inputs from both M1 and M2 (Dudman and Gerfen, 2015; Guo et al., 2015; Hintiryan et al., 2016; Tervo et al., 2016). Both DLS and corticostriatal interactions are known to be important for the learning and control of skilled movements (characterized as fast, accurate, and consistent) in intact individuals (Costa et al., 2004; Yin et al., 2009; Turner and Desmurget, 2010; Shmuelof and Krakauer, 2011; Lemke et al., 2019). Given that stroke survivors are known to demonstrate reduced movement vigor and have an impaired “speed and accuracy” tradeoff (Turnbull et al., 1995; Shmuelof and Krakauer, 2011; Hardwick et al., 2017; Thura and Cisek, 2017), examining how downstream DLS activity changes with recovery of movement speed and task accuracy might be particularly revealing. How might a subcortical region like the DLS, which is a single synapse downstream of M1 in the intact nervous system but also receives sparser projections from M2, change after a focal M1 stroke? Based on the growing evidence for the emergence of stable neural population activity patterns in the corticostriatal network with learning (Lemke et al., 2019), we hypothesized that the coordinated reemergence of reliable single-trial population activity across the PLC and DLS closely tracks recovery of movement control.

We performed chronic dual site multielectrode electrophysiological recordings in PLC and DLS during motor rehabilitation after a focal M1 stroke in rats. Recordings were conducted with high temporal resolution during movement and throughout recovery. Given the growing understanding that neural ensemble dynamics at the level of single trials (not averaged across multiple trials) can better explain complex behaviors (Musall et al., 2019; Veuthey et

al., 2020), we analyzed the local and cross-area ensemble dynamics at both the single-trial and trial-averaged levels. We found that movement-related activity in both PLC and DLS were disrupted after stroke and reorganized together during rehabilitation. Specifically, we observed simultaneous increases in movement modulation of neurons, trial-to-trial reliability of neural patterns, and the ability to decode instantaneous movement speed in PLC and DLS. Fine-timescale coordination of spiking activity between PLC and DLS was also evident with recovery. These increases were significantly correlated with the animals' abilities to perform skilled reaching during rehabilitation. Our results highlight the potential importance of reliable cross-area activations during motor recovery after stroke.

RESULTS

Corticostriatal neural activity was monitored during motor recovery after stroke

We trained Long Evans rats (see Table S1 for total numbers of subjects per group) on a reach-to-grasp task that requires coordination of gross proximal movements and fine distal movements (Figure 1A) using an automated behavior box (Wong et al., 2015). When rats reached plateau performance levels, we induced a photothrombotic stroke over the primary motor cortex forelimb area (Figure 1B). After at least 1 week of recovery from surgery, rats were retrained on the same task as part of physical rehabilitation. In a subset of animals with neural implants, simultaneous *in vivo* electrophysiology recording of neural activity from both PLC and DLS was conducted over this period (n = 8 animals; see STAR Methods; Figures 1B, 1C, S1A, and S1B).

We first assessed whether our PLC recording site (premotor forelimb areas and surrounding areas anterior to M1; Figure S1C) was indeed connected to the DLS recording site. All DLS electrodes were lateral to the midline of the striatum (Figure 1C). We found that the PLC and DLS sites remained functionally (Figure S1D shows short-latency-evoked potentials recorded at the DLS site during PLC stimulation) and physically (Figure 1D shows retrograde labeling at the PLC site when a viral vector was injected in the DLS recording site, and Figure S1E shows the viral injection site in DLS) connected after stroke. This indicated that there was a physical substrate for connectivity that can support possible changes in coupling between PLC and DLS with recovery.

To monitor recovery, we used three behavioral metrics to characterize motor deficits and improvements over time (Figures 1E, 1F, and S2A show behavioral trends for individual animals): pellet retrieval success rate, paw average speed, and speed consistency (correlation of the instantaneous speed change of individual trials with the pre-stroke template). All measures decreased significantly after stroke (Figure 1F; two-tailed paired *t*-test: $t(6) = 8.0947$, $p = 1.9059e\text{-}4$; $t(6) = 5.6853$, $p = 0.0013$; and $t(6) = 13.8028$, $p = 1.4954e\text{-}4$, respectively) and increased significantly with rehabilitation (Figure 2F; linear mixed-effects model: $b = 2.3256$, $t(77) = 6.189$, $p = 2.7235e\text{-}8$; $b = 0.17815$, $t(77) = 7.7367$, $p = 3.2635e\text{-}11$; and $b = 0.01751$, $t(77) = 4.1574$, $p = 8.2784e\text{-}5$, respectively). Success rate did not recover to pre-stroke levels (Figure S2B; two-tailed paired *t*-test: $t(7) = 3.6875$, $p = 0.0078$); notably, lesion size was not significantly correlated with the amount of deficit or recovery in success rate (Figure S2C; Pearson correlation: $r = -0.5606$, $p = 0.1905$; and $r = -0.5352$, $p = 0.1716$ respectively). However, average speed and speed consistency, measures

of gross movements, did recover (Figure S2B; two-tailed paired *t*-test: $t(7) = 0.4931$, $p = 0.5469$; and $t(7) = 2.0343$, $p = 0.0814$, respectively). Reach amplitude, the distance the paw traveled beyond the door toward the pellet, did not change after stroke (two-tailed paired *t*-test: $t(6) = -0.0204$, $p = 0.9844$) or with rehabilitation (linear mixed-effects model: $b = -0.0220$, $t(77) = -0.0709$, $p = 0.9436$). These results show that both fine and gross movements were impaired after a M1 stroke and improved with rehabilitation. However, reach transport and gross aiming to reach the pellet was fully recovered after rehabilitation. Partial recovery of success rate may indicate that either the reach-to-grasp coordination (i.e., timing of grasping relative to reaching is altered) or the grasp itself is impaired.

DLS was partially disrupted but still involved in reaching early after stroke

First, we assessed if DLS activity patterns were altered in the early period after stroke. Even though motor behavior was disrupted in this period, it is possible that DLS activity remained unchanged after stroke and continued to support gross movements (animals were still able to make reaching movement and knock off the pellet). We compared DLS neural activity in rats during the first rehabilitation session post-stroke and in a separate group of control animals (n = 7), i.e., intact animals implanted with electrodes (Figure 2A; Table S1). At the trial-average level, we found that the proportion of movement-modulated DLS units in the stroke rats was lower than that in the intact rats (Figures 2A–2C). Figures 2A and 2B show all neurons and their trial-averaged time course of activity, and Figure 2C shows the proportion of modulated units per animal (two-tailed two-sample *t*-test: $t(11) = 3.2894$, $p = 0.0072$). The distribution of baseline firing rates of units during spontaneous periods (−6 to −3 s relative to trial start) were unchanged (two-sample Kolmogorov-Smirnov test: $D = 0.1906$, $p = 0.0671$). Importantly, only trials in which rats managed to touch the pellet were included in analysis. Further, only trials with durations of less than 0.5 s and with one reach attempt were included (see STAR Methods) to control for intact and stroke animals exhibiting different behaviors. Hence, the decreased proportion of modulated units was not merely due to differences in reaching behaviors between the two groups. Lesion size was also not significantly correlated with the proportion of modulated DLS units (Figure S2D; Pearson correlation: $r = -0.0145$, $p = 0.9783$).

Since DLS neural activity was affected post-stroke, we next asked if DLS was still required for the observed movements post-stroke. These movements primarily comprised reaching attempts that could touch the pellet but did not end with a functional grasp. We implanted infusion cannulas in a separate cohort of stroke rats (n = 4) and inactivated DLS using the GABA agonist muscimol (Figures S3A and S3B) during rehabilitation once rats were able to reach independently. Compared to saline infusions, muscimol inactivation of DLS post-stroke resulted in more variable paw trajectories (Figures S3C and S3D; linear mixed-effects model: $b = 0.5113$, $t(11) = 3.3011$, $p = 0.0071$) and shorter reaches (Figures S3C and S3E; linear mixed-effects model: $b = -0.2047$, $t(11) = -2.7764$, $p = 0.0180$), consistent with previous experiments in healthy animals (Lemke et al., 2019).

In the intact brain, DLS is thought to modulate movement vigor and/or speed (Turner and Desmurget, 2010; Dudman and Krakauer, 2016; Thura and Cisek, 2017; Yttri and Dudman, 2018; Fobbs et al., 2020). Given that DLS was still necessary for some aspects of movement

in stroke animals, we wondered if the remaining DLS neural activity still represented hand speed. We used regularized multiple linear regression to predict instantaneous hand speed from DLS neural activity or shuffled activity (Figure 2D; see STAR Methods). Binned spiking activity at 10 different time lags relative to paw speed was used as input in the decoder. In the fitted regression, different DLS units tended to have high weights at different time lags (Figure 2E), likely related to the general sequential activation of neurons. For each animal, DLS neural activity even in the first rehabilitation session post-stroke predicted arm speed significantly better than chance (Figure 2F). Overall, we found that DLS was partially disrupted after a M1 stroke; despite this, ensemble activity in the DLS still represented movement speed during reaching and was necessary for consistent and high-amplitude movements.

DLS neural dynamics reorganized during rehabilitation

Next, we examined how DLS neural activity patterns changed and whether they tracked motor improvements over rehabilitation. We computed the peri-event time histograms (PETHs) of all units to examine changes at the trial-average level and observed an increase in the proportion of movement-modulated units (Figure 3A). Interestingly, movement-modulated units were initially biased to electrodes in more lateral positions within the DLS multi-electrode array and emerged in more medially located electrodes after rehabilitation (Figure S4A; two-sample t-test comparing medial-lateral positions of modulated units in rehabilitation session 1 and those in session 8: $t(195) = 2.1727$, $p = 0.031$). This suggests that with the loss of M1, there is a change in the topography of DLS task activity. This could be due to changes in the projections from the PLC. Future studies with more detailed and dedicated physiological mapping of the medial-to-lateral density of task activity along with histological quantification of PLC inputs to the striatum are needed to fully understand this apparent shift in medial-lateral location of modulated units.

We also investigated the consistency of single-trial population activity by computing the correlations between single-trial neural activity and the trial-averaged template across all units in a rehabilitation session. In early rehabilitation sessions, trial-to-trial neural firing was inconsistent among kinematically matched trials (Figure 3B). The single-trial to template correlation for non-kinematically matched trials was even lower than that of matched trials (Figure S4B; two-tailed paired t-test: $t(7) = 2.4725$), $p = 0.0427$). However, in later rehabilitation sessions, trials with similar kinematics were consistently associated with a stereotyped sequence of unit activations that also matched the trial-averaged PETH. Across the sessions from all rats, we observed a significant increase in template correlation among matched trials (Figure 3C; linear mixed-effects model: $b = 0.0117$, $t(72) = 5.0044$, $p = 3.8323\text{e-}6$), indicating that trial-to-trial variability in DLS neural activity reduced with recovery. Additionally, template correlation was a significant predictor of task success rate (Figure 3D; linear mixed-effects model: $b = 72.074$, $t(72) = 4.0165$, $p = 0.00014$).

As our past work in the PLC (Ramanathan et al., 2018) suggested a link between single-trial neural firing and low-frequency (1.5–4 Hz) local field potential (LFP) power during movement, we performed the same quantification in DLS. We found that 1.5–4 Hz DLS LFP power, −0.75 to 0.25 s around pellet touch, increased over rehabilitation (linear mixed-

effects model: $b = 0.0141$, $t(75) = 5.6624$, $p = 2.605e\text{-}7$), similar to what we observed previously in PLC during stroke rehabilitation (Ramanathan et al., 2018) and in DLS during motor learning in intact animals (Lemke et al., 2019).

To more directly link the neural changes to behavior, we calculated the paw speed decoding ability of DLS neural activity throughout rehabilitation using the same method as in Figure 2. To account for differences in the number of recorded units across sessions, we subsampled the number of units to the minimum number across all sessions for each rat. Only sessions with at least six units were included in the analysis. To quantify changes across all animals (which have different minimum number of units), the mean decoding r^2 across sessions for each animal was subtracted from the r^2 for each session (Figure S4C shows the mean r^2 for each animal). The decoding r^2 increased with a larger number of units, but the trend across rehabilitation remained the same (Figure S4D). Speed decoding r^2 was positively correlated with rehabilitation session (Figures 3E and 3F; linear mixed-effects model: $b = 0.008491$, $t(72) = 2.8222$, $p = 6.1615e\text{-}3$) and success rate across animals (Figure 3G; linear mixed-effects model: $b = 45.76$, $t(72) = 2.612$, $p = 0.0109$). Although DLS neural activity already represented speed better than chance from the first rehabilitation session (Figure 2F), the relationship between DLS neural activity and paw speed strengthened even more with motor recovery. The improved decoding ability also supports the notion that the neural changes in DLS were not just due to behavioral differences across rehabilitation. Specifically, decoding was done on a moment-by-moment basis for concatenated single trials and hence not influenced by average behavioral differences across sessions. Together, this indicated that DLS activity became more closely tied to arm kinematics during the recovery process.

Changes in PLC activity paralleled changes in DLS

Given the importance of PLC in motor recovery (Nudo and Milliken, 1996; Gharbawie et al., 2007) and our results demonstrating that DLS reorganized with changes in motor behavior, we wondered about the comparative change in PLC. We recorded neural activity from the “future PLC” (i.e., premotor and surrounding regions anterior of M1) and the DLS in the same two groups of animals as in Figure 2 (Figure 4A). Similar to our observations in the DLS, the proportion of movement-modulated units in the PLC was lower in stroke compared to intact animals and increased over rehabilitation (Figure 4B). The single-trial to template correlation in PLC also increased (Figures 4C, 4D, and S4B; linear mixed-effects model: $b = 0.0143$, $t(47) = 6.0579$, $p = 2.1999e\text{-}7$) and was positively correlated with success rate (Figure 4E; linear mixed-effects model: $b = 113.25$, $t(47) = 4.9776$, $p = 9.0736e\text{-}6$). PLC neural activity predicted paw speed better over rehabilitation as well (Figures 4F, 4G, S4C, and S4D; linear mixed-effects model: $b = 0.007355$, $t(47) = 2.6117$, $p = 0.0121$), and speed prediction was positively correlated with success rate (Figure 4H; linear mixed-effects model: $b = 59.13$, $t(47) = 2.61$, $p = 0.039$). The speed decoding performance using PLC units was not significantly different from that using the same number of DLS units or a combination of PLC and DLS units (Figure S4E; repeated-measures ANOVA: $F(2,90) = 0.2699$, $p = 0.7641$). The combined ability of PLC and DLS units together to decode movement speed tended to be between that of PLC units or DLS units only, suggesting that activity in these two regions could compensate for each other. Overall, we found that neural

activity in both PLC and DLS was affected early after stroke and reorganized post-stroke, becoming more movement modulated and less variable.

Neural changes in PLC and DLS occurred simultaneously across rehabilitation sessions

Although we observed similar patterns of reorganization in PLC and DLS, they may or may not occur simultaneously. For example, as PLC is thought to be the primary site of plasticity for stroke recovery, it is possible that reorganization in PLC recruits and drives subsequent changes in downstream areas such as the DLS. If so, we would expect to see reorganization in PLC earlier than that in DLS. We thus directly compared the timescale of neural changes in PLC and DLS by correlating the neural measures (proportion of modulated units, template correlation, and speed decoding ability) on a session-by-session basis at different session lags. Interestingly, we found that the correlation for all neural measures was the highest at zero-session lag (Figures 5A–5C), indicating that PLC and DLS were changing simultaneously instead of one leading or lagging the other. Figure 5D shows the significant positive correlation for template correlation at zero-session lag. Altogether, the results support the idea that PLC and DLS are interdependent throughout rehabilitation and affecting each other's activity through the cortico-basal ganglia loop.

Fine-timescale coordination between PLC and DLS increased after rehabilitation

In the previous sections, our evidence for the close relationship between PLC and DLS was based on session-by-session changes in neural measures local to each area. This does not necessarily indicate that the neural activity patterns in the two structures are coordinated across single trials. Past studies in intact brains have shown that single-trial coordination across cortex and striatum increases during motor learning (Lemke et al., 2019), but it is unknown if this fine-timescale coordination also increases during rehabilitation post-stroke. We first tested LFP coherence between PLC and DLS, as previous studies in intact animals have found increases in M1-DLS theta coherence with learning (Koralek et al., 2013; Lemke et al., 2019). Interestingly, we found that there were instead significant decreases in broadband low-frequency PLC-DLS LFP coherence over time and with recovery (Figures S5A and S5B). This might mean that the two structures are less rhythmically coupled, i.e., because coherence relies on spectral analysis. However, recent studies have indicated that fine-timescale coordination may be evident at the level of spiking (Semedo et al., 2019; Veuthey et al., 2020). Importantly, such methods used statistical methods to measure "communication subspaces" based on ensemble patterns and do not rely on aggregate measures such as the LFP.

Here, we used canonical correlation analysis (CCA) to assess fine-timescale coordination between PLC and DLS during movement (Figure 6A). CCA has been used in various neuroscience studies to extract correlated population activity between two areas (Sussillo et al., 2015; Gallego et al., 2018; Semedo et al., 2019; Veuthey et al., 2020). Specifically, CCA finds a linear combination of units in PLC and DLS that project to PLC and DLS subspaces, respectively, and where activity in these subspaces is maximally correlated (Figure 6B). We used CCA because it allowed us to extract a time series of correlated population activity across two structures, used to analyze coordination at a fine timescale. We used concatenated single-trial spiking activity binned at 100 ms as in a previous paper (Veuthey et al., 2020).

The top component produced by CCA is the axis of the PLC and DLS subspaces that has the maximum correlation between the two areas. We found that this maximum correlation increased with rehabilitation (Figure 6C shows example sessions from a single animal, and Figure 6D shows all sessions from all animal across rehabilitation; linear mixed-effects model: $b = 0.01363$, $t(44) = 4.1562$, $p = 1.4694\text{e-}4$), showing that activity in the two structures became more precisely temporally correlated with recovery. Smaller time bins decreased the canonical correlation but did not change the general trend across rehabilitation (Figures S6A and S6B). Smaller number of units used to compute CCA also resulted in lower correlation but did not change general trend (Figures S6C and S6D). Interestingly, top component activity increased during movement (Figure 6E) and became more movement specific on a trial-by-trial basis after rehabilitation (Figure 6F). This indicated that correlated activity across PLC and DLS was increasingly movement related. The maximum canonical correlation was also a significant predictor of success rate across sessions (linear mixed-effects model: $b = 89.977$, $t(44) = 4.1712$, $p = 1.4017\text{e-}4$). These results highlighted the emergence of fine-timescale coordinated activity between PLC and DLS with rehabilitation of reaching and grasping actions during stroke recovery, in addition to simultaneous changes in neural measures that were local to each area.

DISCUSSION

We investigated how the DLS was affected by a focal M1 stroke and how changes in the DLS are related to reorganization of neural activity patterns in the PLC during the recovery of a dexterous motor skill. DLS activity was partially disrupted in the early recovery period, but it still played a role in the speed and amplitude of reaching movements. With rehabilitation, DLS neural activity became more movement modulated, demonstrated greater trial-to-trial consistency, and better represented movement speed. Similar changes were evident in the PLC and took place simultaneously with DLS. Furthermore, precise temporal coordination of neural activity patterns between PLC and DLS increased over rehabilitation and was correlated with motor recovery. Together, these results demonstrate that recovery of dexterous actions is closely correlated with the emergence of reliable (from trial to trial and with respect to behavior) and precisely aligned neural activity patterns across PLC and DLS. These results, while largely correlative at this stage, can help define precise causal interventions to indicate the specific role that DLS may play in driving recovery.

Effect of cortical stroke on downstream subcortical areas

While a majority of animal studies investigating stroke have focused on the role of cortical structures as primary substrates for recovery of dexterous function (Chollet et al., 1991; Castro-Alamancos and Borrel, 1995; Nudo and Milliken, 1996; Nudo et al., 1996; Gharbawie et al., 2005; Ramanathan et al., 2006; Grefkes and Ward, 2014; Ramanathan et al., 2018; Bönstrup et al., 2019; Latifi et al., 2020; Balbi et al., 2021), lesion and anatomical studies highlight the importance of subcortical areas (Glees and Cole, 1950), including brainstem regions (Zaaimi et al., 2012; Ishida et al., 2016; Darling et al., 2018) and the striatum (Whishaw et al., 1986; Cheng et al., 1997; Karthikeyan et al., 2019). We found that DLS task-related activity patterns were altered early after M1 stroke. As DLS receives most of its inputs from the cortex, this could be due to the loss of motor cortical inputs

and hence insufficient input strength to drive neuronal firing during movement. Moreover, the intriguing finding that there was a medial shift of the striatal task activity with recovery further suggests that understanding the specific projections from PLC to the striatum can be revealing about how DLS specifically contributes to recovery. These findings, together with the observation that activity in both DLS and PLC reorganized in a synchronous manner, suggest that understanding how PLC recruits previously connected areas is important to gain a complete view of the recovery process.

Coordination between PLC and DLS

While PLC has been implicated in recovery of motor function after stroke via descending corticospinal pathways (Ramanathan et al., 2006; Ganguly et al., 2013), it need not have also recruited the striatum using parallel corticostriatal pathways. Our results revealed that behavioral recovery was associated with more consistent sequential activation of neurons in both structures. Furthermore, we found increased fine-timescale alignment of activity between PLC and DLS. What mechanisms might drive the observed changes in cross-area coordination? One possibility is that there are changes in corticostriatal synaptic strength over the recovery process (Yin et al., 2009). There is a large body of literature using largely *in vitro* preparations indicating that long-term potentiation (LTP) can be induced at this connection in an activity-dependent manner (Lerner and Kreitzer, 2011). Alternatively, structural changes (e.g., axon sprouting) could change the strength of corticostriatal connections (Cheng et al., 1997; Carmichael and Chesselet, 2002). It is also possible that a third area is driving changes in both structures or that rehabilitation training modifies the entire motor network simultaneously. To distinguish among these possibilities, future studies could record from other motor areas, such as the contralateral motor cortex, motor thalamus, and cerebellum.

Role of DLS in dexterous motor control post-stroke

A wealth of studies have implicated M1 in the control of gross and fine motor control (Hyland, 1998; Brown and Teskey, 2014; Peters et al., 2014). For fine motor control, descending cortical inputs to brainstem and spinal regions appear to be important both for learning and skilled execution (Esposito et al., 2014; Isa, 2019). In contrast, for isolated gross movements (i.e., reaching movements only), previous work has indicated that very well-trained gross movements can recover after motor cortex injury without further training (Kawai et al., 2015). In our case, consistent with past literature (Ramanathan et al., 2018; Lemke et al., 2019), coordinated gross and fine control was impaired after cortical stroke and slowly recovered with rehabilitation training. The main uncertainty was whether recovery was exclusively a cortical phenomenon. Our results clearly implicate DLS in the recovery process. Since DLS is directly downstream of the PLC, it is possible that it simply receives information from PLC and is not actively engaged in recovery. However, we found that temporary inactivation of DLS perturbed movements, indicating that it is still contributing to movement control. This would not be expected if PLC were the sole site of recovery. Future work can better define the causal role of DLS in the recovery of movement control.

In our previous study in intact animals learning a reach-to-grasp task, we found that gross and fine movement control was linked to different M1 and DLS activity patterns (Lemke et al., 2019). While gross movements were linked to coordinated activity between areas, fine grasping was shown to be more cortically dependent. With DLS inactivation or lesion, proximal movements were altered but the grasping action was not, i.e., animals were able retrieve the pellet when the task was made easier by reducing the transport distance. This suggests that DLS has a role in regulating the timing and the reliability of an action that is composed of multiple sub-movements (Yin et al., 2009; Jin et al., 2014; Markowitz et al., 2018; Lemke et al., 2019). In this study, because of the large behavioral variability in stroke animals, it was not possible to distinguish the different contributions of reaching versus grasping. It is worth noting, however, that the average reach speed and consistency did largely recover back to baseline, while accuracy did not. While it is difficult to determine if the accuracy deficit was due to loss of coordination between reaching and grasp times or simply a deficit of grasping, these findings suggests that gross movement control largely recover while aspects of finer movement control is persistently affected by a M1 stroke.

Implications for stroke rehabilitation and therapies

It is important to point out that the focal M1 stroke model used here is relatively rare from a clinical perspective. More common stroke types include middle cerebral artery (MCA) occlusion, with loss of motor, sensory, and deep white matter and descending pathway lesions in the internal capsule or pons (Ganguly et al., 2013; Grefkes and Ward, 2014; Corbetta et al., 2015). Such lesions affect multiple areas as well as the output pathways to muscles. It is challenging to model this in rodents and interpret what might drive or impede recovery when multiple areas are involved. Given the lack of studies into the electrophysiological correlates of recovery, our approach was to utilize a commonly used experimental model of a focal M1 lesion to study principles of recovery. We are thus able to more precisely map out the network consequence of such an injury. Areas of future investigation include understanding the effects of more extensive lesions that span multiple areas and included connections. This may also be more fruitful in a non-human primate model (Nudo et al., 1996; Khanna et al., 2021), where motor and sensory areas are more compartmentalized and there is more extensive white matter connecting the sensorimotor network.

Our results provide groundwork for future development of therapies that target subcortical and multiple brain areas. We found that motor performance post-stroke could be accounted by the extent of coordinated activity between cortex and striatum. Poor recovery in some animals may be related to weaker neurophysiological coupling between PLC and DLS after stroke, in comparison to the intact M1 and striatum. Increasing structural or functional connectivity between PLC and DLS, for example through electrical stimulation (Ramanathan et al., 2018; Khanna et al., 2021), might further improve speed, consistency, and accuracy. Subcortical areas like DLS are also attractive targets for neuromodulation, as they are more compact and hence easier to target than the cortex and have widespread connections throughout the brain (Perlmutter and Mink, 2006).

Interestingly, there is also a long history of testing dopamine agonists in clinical stroke populations (Cramer, 2015), but the precise mechanism remains unclear. Our results suggest possible mechanisms for this treatment approach. It is known that dopamine activation during training can aid action selection and ultimately result in consolidated skilled actions (Lerner and Kreitzer, 2011; Markowitz et al., 2018). Our finding showing that corticostriatal interactions are important for recovery suggests a more direct link. Future studies can determine how dopamine dynamics directly impact recovery and suggest approaches to optimize dopamine agonist treatment, such as whether treatments should be given only during rehabilitation training or in a continuous manner such that it impacts the offline processing that is essential for skill consolidation (Gulati et al., 2017; Kim et al., 2019).

STAR★METHODS

RESOURCE AVAILABILITY

Lead contact—Further information and requests for resources and reagents should be directed to and will be fulfilled by the Lead Contact, Karunesh Ganguly (karunesh.ganguly@ucsf.edu).

Materials availability—This study did not generate new unique reagents.

Data and code availability—The datasets and code supporting the current study have not been deposited in a public repository because they are still being used for current studies, but are available from the corresponding author upon reasonable request.

EXPERIMENTAL MODEL AND SUBJECT DETAILS

All procedures were in accordance with protocols approved by the Institutional Animal Care and Use Committee at the San Francisco Veterans Affairs Medical Center. Adult male Long Evans rats (n = 23, 250–400 g; Charles River Laboratories; see Table S1 for the number of rats used in each experiment) were housed in a 12-h/12-h light–dark cycle. All experiments were done during the light cycle. Animals were pair-housed prior to electrode/cannula implantation and then singly housed after to prevent damage to implants. If applicable, animals were randomly assigned to experimental groups.

METHOD DETAILS

Animal care and surgery—All surgical procedures were performed using sterile techniques under 2%–4% isoflurane. Surgery involved cleaning and exposure of the skull and preparation of the skull surface using cyanoacrylate and then implantation of the skull screws for referencing and overall head-stage stability. The postoperative recovery regimen included the administration of 0.02 mg per kg body weight buprenorphine for 2 days, and 0.2 mg per kg body weight meloxicam, 0.5 mg per kg body weight dexamethasone and 15 mg per kg body weight trimethoprim sulfadiazine for 5 days. All animals were allowed to recover for 1 week prior to further behavioral training.

Surgery for electrophysiology recordings—Reference and ground screws were implanted posterior to lambda, ipsilateral and contralateral, respectively, to the neural

recordings. Craniotomy and durectomy were performed, followed by stroke induction (if any) and then implantation of the neural probes. We used either 32- or 64-channel arrays (33/35-μm polyamide-coated tungsten microwire arrays, Tucker-Davis Technologies and Innovative Neurophysiology). Arrays targeting the perilesional cortex were centered at 4mm anterior and 2 mm lateral to the bregma and lowered to a depth of 1.5mm from the brain surface, and arrays targeting the dorsolateral striatum were centered at 0.5mm anterior and 4mm lateral to bregma and lowered to a depth of 4mm from the brain surface. The final locations of electrodes were confirmed by electrolytic lesions.

Photothrombotic stroke—After craniotomy, rose bengal dye was injected into the femoral vein using an intravenous catheter. Next, the surface of the brain was illuminated with white light (KL-1500 LCD, Schott) using a fiber optic cable for 20 min. We used a 4-mm aperture for stroke induction, centered at 3mm lateral and 0.5mm anterior to bregma, and covered the remaining cortical area with a custom aluminum foil mask to prevent light penetration. If no neural probes were needed, the craniotomy was covered with a layer of silicone (Kwik-Sil) and the incision was closed with sutures.

Surgery for infusions—After craniotomy and stroke induction, cannulas (PlasticsOne) were implanted to target the DLS (same coordinates as electrode arrays). The location and spread of muscimol was determined by infusing a fluorescent muscimol (Invitrogen BODIPY TMR-X Conjugate) right before perfusion and histology.

Viral injection—750–1500nl of retrogradeAAV-hSyn-JAWs-KGC-GFP-ER2 (Addgene) (Tervo et al., 2016) was injected in the DLS (same coordinates as before) of 3 stroke rats, using a Hamilton syringe and needle. Injection was performed one week after stroke induction. Rats used for viral injection were not trained on the reach-to-grasp task. 4 weeks after viral injection, rats were anesthetized and perfused as described in the immunohistochemistry section.

Electrolytic lesion—Rats were anesthetized with 2% isoflurane and electrical current (−300 μA for 10 s) was passed through every channel, 2 at a time, of the implanted electrode arrays using the TDT IZ2 system. Rats were perfused right after the electrolytic lesions were completed.

Immunohistochemistry—After all experiments, rats were anesthetized and transcardially perfused with 0.9% sodium chloride, followed by phosphate-buffered 4% formaldehyde (PFA). The harvested brains were post-fixed for 24 h and immersed in 20% sucrose for 2 days. NeuN staining was used for stroke and electrode localization. Coronal cryostat sections (40-μ m thickness) were incubated with blocking buffer (10% Donkey serum and 0.1% Triton X-100 in 0.1 M phosphate buffer) for 1 hour and then incubated overnight with mouse anti-NeuN (MAB377, 1:1000, Millipore, Temecula, CA, USA). After washing, the sections were incubated with biotinylated anti-mouse IgG secondary antibody (BA-9200, 1:250, Vector Lab, Burlingame, CA, USA) for 2 hours. Sections were incubated with avidin–biotin peroxidase complex reagents using a Vector ABC kit (Vector Labs). The horseradish peroxidase reaction was detected with diaminobenzidine and H_2O_2 using DAB substrate kit (SK-4100, Vector Lab, Burlingame, CA, USA). The sections were washed

in phosphate buffer and then mounted with permount solution (Fisher Scientific) on superfrosted coated slides (Fisher Scientific). Images of whole sections with NeuN staining were taken by a HP scanner.

For the quantification of the infarct volume, brain sections spaced 480 μm apart spanning the entire infarct region were imaged by Leica stereo microscope (LEICA M205 C, Leica microsystems Inc., Buffalo grove, IL, USA). The area of neuronal loss in each section was calculated in ImageJ software and infarct volumes were expressed as a percentage of the non-ischemic hemisphere as described in Swanson et al. (1990).

For fluorescent imaging (viral tracing and muscimol localization), 40um sections were mounted directly with mounting media containing DAPI (VectorShield). Fluorescent images were taken by a Zeiss microscope.

***In vivo* electrophysiology—**Units and LFP activity were recorded using a 128-channel TDT-RZ2 system (Tucker-Davis Technologies). Spike data were sampled at 24,414 Hz and LFP data at 1,017.3 Hz. ZIF clip-based analog head stages with a unity gain and high impedance (~1 GΩ) were used. The threshold for spiking activity was set online using a standard deviation of 4.5 (calculated over a 1-min period using the TDT-RZ2 system), and waveforms and timestamps were stored for any event that crossed that threshold. Sorting was performed using Plexon OfflineSorter v4.3.0, using a principal component analysis (PCA)-based method followed by manual inspection and sorting. We included both clearly identified single-units and multi-unit activity for this analysis (results were pooled as there were not clear differences in single-unit and multi-unit responses). Behavior-related timestamps (trial onset and trial completion) were sent to the RZ2 analog input channel using an Arduino digital board and synchronized to neural data.

Evoked potentials—To probe the functional connectivity between PLC and DLS, we measured short latency evoked potentials in DLS from PLC stimulation in 3 of the 8 chronically implanted stroke animals. This was done after all rehabilitation and electrophysiology recordings were completed. While animals were awake and resting, biphasic pulses (20–100 μA, 200 μs per phase with 100 μs inter-phase interval, 5 pulses per current condition, Tucker Davis Technologies (TDT), IZ2) were applied in PLC at four tungsten microwire array electrodes (TDT, ~50 kOhm input impedance at 1000 Hz) with recording of DLS LFP short-latency evoked potentials (5–10ms after stimulation offset) in all striatal array channels (TDT, PZ2). DLS LFP was median-referenced, without z-scoring, and trials with motion artifact were excluded. Evoked response was averaged for each current amplitude condition and tested again two weeks later to confirm mapping stability. Channel pairs that demonstrated increased short-latency EP amplitude with increased current injection were deemed to reflect monosynaptic connections.

Intra-cortical microstimulation (ICMS) mapping—We conducted ICMS motor mapping in an intact animal not used for other experiments to confirm placement location of the PLC/M2 array and that movements can be evoked from the PLC/M2 area. This animal was anesthetized with a mixture of ketamine (100 mg/kg) and xylazine (16.67 mg/kg) delivered intraperitoneally. Supplementary 0.5–1ml doses of the mixture were provided as

needed, based on toe pinch response. 32-channel multi-electrode arrays (TDT), the same type of electrodes we used for chronic *in vivo* electrophysiology were implanted in the PLC/M2 area (+4mm anterior and +2mm lateral from bregma) at a depth of 1.5mm from the brain surface. Triplet biphasic trains of 200 μs per phase (100 μs interphase interval, 333Hz triplet) were delivered at each electrode using a constant current stimulator (IZ2, TDT). The trains were delivered with 50–150 μA amplitude. Stimulation was delivered to each electrode in the array with video recording of forelimb at 20Hz.

Behavior

Training: Rats were acclimated to the behavioral box for at least 2 days and then trained to a plateau level of performance (> 50% success rate for 4 consecutive days, Figure 1F shows pre-stroke baseline values) in a reach-to-grasp task before neural probe implantation. Rats typically took 1 to 2 weeks of daily training (~100 trials per day) to reach plateau performance. Probe implantation was performed contralateral to the preferred hand. Rats were allowed to recover for at least 5 days before the start of experimental sessions. During behavioral assessments, we monitored the animals and ensured that their body weights did not drop below 90% of their initial weight. We used an automated reach-box, controlled by custom MATLAB scripts and an Arduino microcontroller. This setup requires minimal user intervention, as described previously (Wong et al., 2015). Each trial consisted of a pellet dispensed on the pellet tray, followed by an alerting beep indicating that the trial was beginning. Rats had to first move to the back of the box, breaking an infrared sensor which opens the door to the pellet. They then had 20 s to reach their arms through the slot, grasp and retrieve the pellet. A real-time 'pellet detector' using an infrared detector centered over the pellet was used to determine when the pellet was moved, which indicated that the trial was over and the door was closed. All trials were captured by video through a camera placed on the side of the behavioral box. The camera was synced with the electrophysiology data either using Arduino digital output or directly through TTL pulses to the TDT RZ2 system. The video frame rate was 65–75 Hz.

Stroke rehabilitation: Rats began rehabilitation training 5–7 days after surgery by performing the same reach-to-grasp task. Electrophysiology recordings began after rats were able to reach independently without experimenter prompting. Rehabilitation training consisted of one to two sessions of 100–150 trials per day for 7–12 days. Sessions within a day were spaced by at least 2 hours. Rehabilitation training was stopped when single units could no longer be reliably recorded.

Muscimol experiments: After stroke induction and recovery from surgery, rats (n = 4) were trained in the same reach-to-grasp task (2 sessions of 100 trials per day, spaced by 3 hours) until they can reach independently (perform task without prompting from experimenter) and achieved a success rate of at least 20%. Infusions began after these criteria were met. On each infusion day, rats first performed a baseline session of 100 trials. They were then anesthetized with 2% isoflurane and injected with 100–400nl (1 μg/μl) of the GABA receptor agonist muscimol (Tocris Bioscience) or equal volume of saline (0.9% sodium chloride) into the dorsolateral striatum. Injection was done at a rate of 100nl/min through a chronically implanted cannula (PlasticsOne) using a Hamilton infusion syringe. The infusion

syringe was left in place for 10 minutes post-infusion. Rats were allowed to recover for 2 hours in their home cage before starting the next session of 100 trials. Muscimol and saline infusion days were alternated for each animal and randomized across animals.

QUANTIFICATION AND STATISTICAL ANALYSIS

Behavioral analysis—Behavioral analysis was done based on video recorded during experimental sessions. The rats' dominant paws were painted with an orange marker at the beginning of each session to facilitate tracking of their paw positions. Reach videos were viewed and semi-automatically scored to obtain trial success, hand position and time points for reach onset, pellet touch and retract onset. To characterize motor performance, we quantified pellet retrieval success rate (percentage of pellets successfully retrieved into the box), average paw speed (average speed from reach onset, the start of the last paw advancement toward the pellet, to time of pellet touch) and speed consistency (median correlation between single trial instantaneous paw speed from 0.4 s to 0.05 s around pellet touch and the median paw instantaneous speed before stroke/ infusion). Only trials in which the rat touched or knocked off the pellet were included in analysis. In muscimol experiments, we also quantified paw position variability (the closest euclidean distance between paw position in each frame and the mean paw trajectory) and reach amplitude (the farthest distance the paw traveled beyond the slot).

Neural data analysis

Analyses were conducted using custom-written scripts and functions in MATLAB 2018b (MathWorks). Sessions with no spiking activity were excluded from analysis (2 rats had no PLC activity throughout rehabilitation and were excluded from PLC analyses, 1 rat had no PLC or DLS activity in the first two rehabilitation sessions).

Trial matching

For unit modulation and trial to template neural correlation analyses, only trials with one reach attempt and a reach to pellet touch duration of < 0.5 s were included. This was to account for the differences in behavioral variability across sessions.

Unit modulation

Spikes were binned at 20ms and time locked to behavioral markers. For visualization purposes, the peri-event time histogram (PETH) was estimated by Bayesian adaptive regression splines (Wallstrom et al., 2008). To determine if a unit was significantly modulated during movement, circular shuffling was performed on the binned firing rate data (without spline fitting). The firing rate from −2 to 2 s around pellet touch for each trial of a unit was shifted circularly by a random time. The PETH was then recomputed from the shuffled data and the mean squared error (the difference between the firing rate in each bin and the mean across all bins from −2 to 2 s around pellet touch) of the PETH was calculated. This was repeated 5000 times to obtain a distribution of mean squared error values. The actual mean squared error of the real PETH was compared to this distribution to obtain a p value. A p value of < 0.05, after bonferroni correction for multiple comparisons, was considered significant.

Single trial to template correlation

Spikes from −2 s to 2 s around pellet touch were binned at 20ms, smoothed with a Gaussian kernel with a standard deviation of 60ms and then z-scored. Binned, smoothed and standardized spike counts for all units of a single trial were then concatenated into one long vector. The correlation (measured using Pearson's r) between each concatenated single trial neural activity and the mean template (mean of all trials excluding current trial) was computed and the median correlation for each session was reported. To account for different numbers of units across rehabilitation sessions, units were subsampled to the lowest number across sessions for each animal (units were randomly sub-selected and the template correlation was recomputed 1000 times). Only sessions with at least 6 units were included.

Speed decoding

A multiple linear regression with LASSO (Least Absolute Shrinkage and Selection Operator) regularization was used to predict paw speed, using PLC or DLS spiking activity. The regression was implemented using the MATLAB function *fitrlinear*. Spikes were binned at 20ms and instantaneous paw speed from the first reach to the last retract of each trial was interpolated to match the neural time bin. Predictors were binned spike counts of units at 10 time lags, spaced equally from 0 to −180ms relative to paw speed. Speed decoding r^2, the proportion of variance in instantaneous speed that was explained by neural activity, was computed using 5-fold cross validation. In each fold, 80% of the data was used for regularization parameter lambda selection and regression fitting, and 20% of the data was used for testing/computing r^2. The regularization parameter lambda was determined using 5-fold cross validation using the training data only (80% of the total data). The lambda value that gave the lowest mean squared error was used for model fitting. For a fairer comparison of r^2 values across different rehabilitation sessions with different numbers of units, units were subsampled to the lowest number of units across sessions (units were randomly sub-selected 500 times). Only sessions with at least 6 units were included. To obtain a chance level of decoding performance, neural activity was shuffled relative to paw speed (e.g., trial 1's speed is matched with trial 5′s neural activity) and r^2 was recomputed the same way as above.

Session by session cross-correlation between PLC and DLS

The correlation between PLC and DLS neural measures (proportion of modulated units, trial to mean neural correlation and speed decoding) were calculated at different time lags, by shifting the DLS measure by −2, −1, 0, +1 and +2 rehabilitation sessions relative to the PLC measures. If the lagged DLS/PLC session did not have a matching PLC/DLS session, the session was removed from analysis, instead of padding the other session. To obtain the shuffled null distribution, we randomly permuted the sequence of the sessions within each animal and recalculated the cross-correlation across all sessions from all animals 1000 times.

Canonical correlation analysis (CCA)

CCA identifies maximally correlated linear combinations between two groups of variables. Unit spiking data in PLC and DLS from −1.5 s to 1.5 s around pellet touch for each trial were binned at 100ms and concatenated. CCA models were then fit using the MATLAB

function *canoncorr*. Only the top canonical component was used in this paper. Only sessions with at least 6 units in both PLC and DLS were included. To account for different numbers of units across rehabilitation sessions, PLC and DLS units were subsampled to the lowest number across sessions for each animal.

Local field potential (LFP) analyses

Artifact reject was first performed on LFP signals to remove broken channels and noisy trials. LFPs were then z-scored and median referenced separately for PLC and DLS. There were no detected PLC units in 2 of the 8 animals with simultaneous PLC and DLS recordings post-stroke. Hence, the PLC LFP activity from those two animals were excluded from analysis. LFP power was calculated on a trial-by-trial basis and then averaged across channels and animals, with wavelet decomposition using the EEGLAB function *newtimef*. PLC-DLS LFP coherence was calculated for each pair of channels using the Chronux function *cohgramc* with 0.75 s windows moving by 0.01 s.

Statistical analysis

Parametric statistics were generally used in this study (t test, ANOVA, Pearson's correlation and linear regression). Details are described in the text under the results section and/or in the figure legends. All statistical analyses were implemented within MATLAB. The linear mixed-effects model (implemented using MATLAB *fitlme*) was used to compare the differences in behavior, trial to mean correlation, speed decoding and canonical correlation. This model accounts for the fact that units or sessions from the same animal are more correlated than those from different animals and is more stringent than computing statistical significance over all units and sessions. We fitted random intercepts for each rat and reported the p values for the regression coefficients associated with muscimol or saline, pre-stroke or post-stroke, or rehabilitation session.

Supplementary Material

Refer to Web version on PubMed Central for supplementary material.

ACKNOWLEDGMENTS

The research described here was supported by the Department of Veterans Affairs; the Veterans Health Administration, Rehabilitation Research and Development Service (award 1I01RX001640); the National Institute of Neurological Disorders and Stroke of the National Institutes of Health (award K02NS093014); and the National Institute of Mental Health (award R01MH111871). K.G. holds a Career Award for Medical Scientists from the Burroughs Wellcome Fund. L.G. was supported by a fellowship from A*STAR, Singapore. S.M.L. was supported by a fellowship from the American Heart Association. S.K. was supported by a fellowship from the National Institute of Neurological Disorders and Stroke, United States (award 1F31NS117010-01A1).

REFERENCES

Balbi M, Xiao D, Jativa Vega M, Hu H, Vanni MP, Bernier LP, LeDue J, MacVicar B, and Murphy TH (2021). Gamma frequency activation of inhibitory neurons in the acute phase after stroke attenuates vascular and behavioral dysfunction. Cell Rep. 34, 108696. [PubMed: 33535035]

Baudat C, Maréchal B, Corredor-Jerez R, Kober T, Meuli R, Hagmann P, Michel P, Maeder P, and Dunet V (2020). Automated MRI-based volumetry of basal ganglia and thalamus at the chronic phase of cortical stroke. Neuroradiology 62, 1371–1380. [PubMed: 32556424]

Bönstrup M, Krawinkel L, Schulz R, Cheng B, Feldheim J, Thomalla G, Cohen LG, and Gerloff C (2019). Low-Frequency Brain Oscillations Track Motor Recovery in Human Stroke. Ann. Neurol. 86, 853–865. [PubMed: 31604371]

Brown AR, and Teskey GC (2014). Motor cortex is functionally organized as a set of spatially distinct representations for complex movements. J. Neurosci. 34, 13574–13585. [PubMed: 25297087]

Buzsáki G (2010). Neural Syntax: Cell Assemblies, Synapsembles, and Readers. Neuron 68, 362–385. [PubMed: 21040841]

Carmichael ST, and Chesselet M-F (2002). Synchronous neuronal activity is a signal for axonal sprouting after cortical lesions in the adult. J. Neurosci. 22, 6062–6070. [PubMed: 12122067]

Carrera E, and Tononi G (2014). Diaschisis: past, present, future. Brain 137, 2408–2422. [PubMed: 24871646]

Castro-Alamancos MA, and Borrel J (1995). Functional recovery of forelimb response capacity after forelimb primary motor cortex damage in the rat is due to the reorganization of adjacent areas of cortex. Neuroscience 68, 793–805. [PubMed: 8577374]

Cheng HW, Rafols JA, Goshgarian HG, Anavi Y, Tong J, and McNeill TH (1997). Differential spine loss and regrowth of striatal neurons following multiple forms of deafferentation: a Golgi study. Exp. Neurol. 147, 287–298. [PubMed: 9344554]

Chollet F, DiPiero V, Wise RJ, Brooks DJ, Dolan RJ, and Frackowiak RS (1991). The functional anatomy of motor recovery after stroke in humans: a study with positron emission tomography. Ann. Neurol. 29, 63–71. [PubMed: 1996881]

Corbett D, Carmichael ST, Murphy TH, Jones TA, Schwab ME, Jolkkonen J, Clarkson AN, Dancause N, Weiloch T, Johansen-Berg H, et al. (2017). Enhancing the Alignment of the Preclinical and Clinical Stroke Recovery Research Pipeline: Consensus-Based Core Recommendations From the Stroke Recovery and Rehabilitation Roundtable Translational Working Group. Neurorehabil. Neural Repair 31, 699–707. [PubMed: 28803530]

Corbetta M, Ramsey L, Callejas A, Baldassarre A, Hacker CD, Siegel JS, Astafiev SV, Rengachary J, Zinn K, Lang CE, et al. (2015). Common behavioral clusters and subcortical anatomy in stroke. Neuron 85, 927–941. [PubMed: 25741721]

Costa RM, Cohen D, and Nicolelis MAL (2004). Differential corticostriatal plasticity during fast and slow motor skill learning in mice. Curr. Biol. 14, 1124–1134. [PubMed: 15242609]

Cramer SC (2008). Repairing the human brain after stroke: I. Mechanisms of spontaneous recovery. Ann. Neurol. 63, 272–287. [PubMed: 18383072]

Cramer SC (2015). Drugs to Enhance Motor Recovery After Stroke. Stroke 46, 2998–3005. [PubMed: 26265126]

Darling WG, Ge J, Stilwell-Morecraft KS, Rotella DL, Pizzimenti MA, and Morecraft RJ (2018). Hand Motor Recovery Following Extensive Fronto-parietal Cortical Injury Is Accompanied by Upregulated Corticoreticular Projections in Monkey. J. Neurosci. 38, 6323–6339. [PubMed: 29899028]

Doyon J, and Benali H (2005). Reorganization and plasticity in the adult brain during learning of motor skills. Curr. Opin. Neurobiol. 15, 161–167. [PubMed: 15831397]

Dudman JT, and Gerfen CR (2015). The Basal Ganglia. The Rat Nervous System (Elsevier), pp. 391–440.

Dudman JT, and Krakauer JW (2016). The basal ganglia: From motor commands to the control of vigor. Curr. Opin. Neurobiol. 37, 158–166. [PubMed: 27012960]

Esposito MS, Capelli P, and Arber S (2014). Brainstem nucleus MdV mediates skilled forelimb motor tasks. Nature 508, 351–356. [PubMed: 24487621]

Fobbs WC, Bariselli S, Licholai JA, Miyazaki NL, Matikainen-Ankney BA, Creed MC, and Kravitz AV (2020). Continuous Representations of Speed by Striatal Medium Spiny Neurons. J. Neurosci. 40, 1679–1688. [PubMed: 31953369]

Gallego JA, Perich MG, Naufel SN, Ethier C, Solla SA, and Miller LE (2018). Cortical population activity within a preserved neural manifold underlies multiple motor behaviors. Nat. Commun. 9, 4233. [PubMed: 30315158]

Ganguly K, Byl NN, and Abrams GM (2013). Neurorehabilitation: motor recovery after stroke as an example. Ann. Neurol. 74, 373–381. [PubMed: 25813243]

Gharbawie OA, Gonzalez CL, Williams PT, Kleim JA, and Whishaw IQ (2005). Middle cerebral artery (MCA) stroke produces dysfunction in adjacent motor cortex as detected by intracortical microstimulation in rats. Neuroscience 130, 601–610. [PubMed: 15590144]

Gharbawie OA, Karl JM, and Whishaw IQ (2007). Recovery of skilled reaching following motor cortex stroke: do residual corticofugal fibers mediate compensatory recovery? Eur. J. Neurosci. 26, 3309–3327. [PubMed: 18028116]

Glees P, and Cole J (1950). Recovery of skilled motor functions after small repeated lesions of motor cortex in macaque. J. Neurophysiol. 13, 137–148.

Grefkes C, and Ward NS (2014). Cortical reorganization after stroke: how much and how functional? Neuroscientist 20, 56–70. [PubMed: 23774218]

Gulati T, Guo L, Ramanathan DS, Bodepudi A, and Ganguly K (2017). Neural reactivations during sleep determine network credit assignment. Nat. Neurosci. 20, 1277–1284. [PubMed: 28692062]

Guo Q, Wang D, He X, Feng Q, Lin R, Xu F, Fu L, and Luo M (2015). Whole-brain mapping of inputs to projection neurons and cholinergic interneurons in the dorsal striatum. PLoS ONE 10, e0123381. [PubMed: 25830919]

Hardwick RM, Rajan VA, Bastian AJ, Krakauer JW, and Celnik PA (2017). Motor Learning in Stroke: Trained Patients Are Not Equal to Untrained Patients With Less Impairment. Neurorehabil. Neural Repair 31, 178–189. [PubMed: 27789762]

Hintiryan H, Foster NN, Bowman I, Bay M, Song MY, Gou L, Yamashita S, Bienkowski MS, Zingg B, Zhu M, et al. (2016). The mouse corticostriatal projectome. Nat. Neurosci. 19, 1100–1114. [PubMed: 27322419]

Houk JC, and Wise SP (1995). Feature Article: Distributed Modular Architectures Linking Basal Ganglia, Cerebellum, and Cerebral Cortex: Their Role in Planning and Controlling Action. Cereb. Cortex 5, 95–110. [PubMed: 7620294]

Hyland B (1998). Neural activity related to reaching and grasping in rostral and caudal regions of rat motor cortex. Behav. Brain Res. 94, 255–269. [PubMed: 9722277]

Isa T (2019). Dexterous Hand Movements and Their Recovery After Central Nervous System Injury. Annu. Rev. Neurosci. 42, 315–335. [PubMed: 30939102]

Ishida A, Isa K, Umeda T, Kobayashi K, Kobayashi K, Hida H, and Isa T (2016). Causal Link between the Cortico-Rubral Pathway and Functional Recovery through Forced Impaired Limb Use in Rats with Stroke. J. Neurosci. 36, 455–467. [PubMed: 26758837]

Jin X, Tecuapetla F, and Costa RM (2014). Basal ganglia subcircuits distinctively encode the parsing and concatenation of action sequences. Nat. Neurosci. 17, 423–430. [PubMed: 24464039]

Karthikeyan S, Jeffers MS, Carter A, and Corbett D (2019). Characterizing Spontaneous Motor Recovery Following Cortical and Subcortical Stroke in the Rat. Neurorehabil. Neural Repair 33, 27–37. [PubMed: 30526316]

Kawai R, Markman T, Poddar R, Ko R, Fantana AL, Dhawale AK, Kampff AR, and Ölveczky BP (2015). Motor cortex is required for learning but not for executing a motor skill. Neuron 86, 800–812. [PubMed: 25892304]

Khanna P, Totten D, Novik L, Roberts J, Morecraft RJ, and Ganguly K (2021). Low-frequency stimulation enhances ensemble co-firing and dexterity after stroke. Cell 184, 912–930.e20. [PubMed: 33571430]

Kim J, Gulati T, and Ganguly K (2019). Competing Roles of Slow Oscillations and Delta Waves in Memory Consolidation versus Forgetting. Cell 179, 514–526.e13. [PubMed: 31585085]

Koralek AC, Costa RM, and Carmena JM (2013). Temporally precise cell-specific coherence develops in corticostriatal networks during learning. Neuron 79, 865–872. [PubMed: 23954030]

Latifi S, Mitchell S, Habibey R, Hosseini F, Donzis E, Estrada-Sánchez AM, Nejad HR, Levine M, Golshani P, and Carmichael ST (2020). Neuronal network topology indicates distinct recovery processes after stroke. Cereb. Cortex 30, 6363–6375. [PubMed: 32728724]

Lemke SM, Ramanathan DS, Guo L, Won SJ, and Ganguly K (2019). Emergent modular neural control drives coordinated motor actions. Nat. Neurosci. 22, 1122–1131. [PubMed: 31133689]

Lerner TN, and Kreitzer AC (2011). Neuromodulatory control of striatal plasticity and behavior. Curr. Opin. Neurobiol. 21, 322–327. [PubMed: 21333525]

Liu A, Vöröslakos M, Kronberg G, Henin S, Krause MR, Huang Y, Opitz A, Mehta A, Pack CC, Krekelberg B, et al. (2018). Immediate neurophysiological effects of transcranial electrical stimulation. Nat. Commun. 9, 5092. [PubMed: 30504921]

Markowitz JE, Gillis WF, Beron CC, Neufeld SQ, Robertson K, Bhagat ND, Peterson RE, Peterson E, Hyun M, Linderman SW, et al. (2018). The Striatum Organizes 3D Behavior via Moment-to-Moment Action Selection. Cell 174, 44–58.e17. [PubMed: 29779950]

Musall S, Kaufman MT, Juavinett AL, Gluf S, and Churchland AK (2019). Single-trial neural dynamics are dominated by richly varied movements. Nat. Neurosci. 22, 1677–1686. [PubMed: 31551604]

Nudo RJ, and Milliken GW (1996). Reorganization of movement representations in primary motor cortex following focal ischemic infarcts in adult squirrel monkeys. J. Neurophysiol. 75, 2144–2149. [PubMed: 8734610]

Nudo RJ, Wise BM, SiFuentes F, and Milliken GW (1996). Neural substrates for the effects of rehabilitative training on motor recovery after ischemic infarct. Science 272, 1791–1794. [PubMed: 8650578]

Perlmutter JS, and Mink JW (2006). Deep brain stimulation. Annu. Rev. Neurosci. 29, 229–257. [PubMed: 16776585]

Peters AJ, Chen SX, and Komiyama T (2014). Emergence of reproducible spatiotemporal activity during motor learning. Nature 510, 263–267. [PubMed: 24805237]

Peters AJ, Steinmetz NA, Harris KD, and Carandini M (2019). Striatal activity reflects cortical activity patterns. bioRxiv. 10.1101/703710.

Ramanathan D, Conner JM, and Tuszynski MH (2006). A form of motor cortical plasticity that correlates with recovery of function after brain injury. Proc. Natl. Acad. Sci. USA 103, 11370–11375. [PubMed: 16837575]

Ramanathan DS, Guo L, Gulati T, Davidson G, Hishinuma AK, Won SJ, Knight RT, Chang EF, Swanson RA, and Ganguly K (2018). Low-frequency cortical activity is a neuromodulatory target that tracks recovery after stroke. Nat. Med. 24, 1257–1267. [PubMed: 29915259]

Rüber T, Schlaug G, and Lindenberg R (2012). Compensatory role of the cortico-rubro-spinal tract in motor recovery after stroke. Neurology 79, 515–522. [PubMed: 22843266]

Sauerbrei BA, Guo JZ, Cohen JD, Mischiati M, Guo W, Kabra M, Verma N, Mensh B, Branson K, and Hantman AW (2020). Cortical pattern generation during dexterous movement is input-driven. Nature 577, 386–391. [PubMed: 31875851]

Semedo JD, Zandvakili A, Machens CK, Yu BM, and Kohn A (2019). Cortical Areas Interact through a Communication Subspace. Neuron 102, 249–259.e4. [PubMed: 30770252]

Shmuelof L, and Krakauer JW (2011). Are we ready for a natural history of motor learning? Neuron 72, 469–476. [PubMed: 22078506]

Sussillo D, Churchland MM, Kaufman MT, and Shenoy KV (2015). A neural network that finds a naturalistic solution for the production of muscle activity. Nat. Neurosci. 18, 1025–1033. [PubMed: 26075643]

Swanson RA, Morton MT, Tsao-Wu G, Savalos RA, Davidson C, and Sharp FR (1990). A Semiautomated Method for Measuring Brain Infarct Volume. J. Cereb. Blood Flow Metab. 10, 290–293. [PubMed: 1689322]

Tervo DGR, Hwang BY, Viswanathan S, Gaj T, Lavzin M, Ritola KD, Lindo S, Michael S, Kuleshova E, Ojala D, et al. (2016). A Designer AAV Variant Permits Efficient Retrograde Access to Projection Neurons. Neuron 92, 372–382. [PubMed: 27720486]

Thura D, and Cisek P (2017). The Basal Ganglia Do Not Select Reach Targets but Control the Urgency of Commitment. Neuron 95, 1160–1170. [PubMed: 28823728]

Turnbull GI, Charteris J, and Wall JC (1995). A comparison of the range of walking speeds between normal and hemiplegic subjects. Scand. J. Rehabil. Med. 27, 175–182. [PubMed: 8602480]

Turner RS, and Desmurget M (2010). Basal ganglia contributions to motor control: a vigorous tutor. Curr. Opin. Neurobiol. 20, 704–716. [PubMed: 20850966]

Veuthey TL, Derosier K, Kondapavulur S, and Ganguly K (2020). Single-trial cross-area neural population dynamics during long-term skill learning. Nat. Commun. 11, 4057. [PubMed: 32792523]

von Monakow C (1914). Lokalisation im Gehirn und Funktionelle Sta'rungen Induziert Durch Kortikale Läsionen (Bergmann JF).

Vyas S, Golub MD, Sussillo D, and Shenoy KV (2020). Computation through Neural Population Dynamics. Annu. Rev. Neurosci. 43, 249–275. [PubMed: 32640928]

Wagner MJ, Kim TH, Kadmon J, Nguyen ND, Ganguli S, Schnitzer MJ, and Luo L (2019). Shared Cortex-Cerebellum Dynamics in the Execution and Learning of a Motor Task. Cell 177, 669–682.e24. [PubMed: 30929904]

Wallstrom G, Liebner J, and Kass RE (2008). An Implementation of Bayesian Adaptive Regression Splines (BARS) in C with S and R Wrappers. J. Stat. Softw. 26, 1–21. [PubMed: 19777145]

Ward NS, Brown MM, Thompson AJ, and Frackowiak RS (2003). Neural correlates of motor recovery after stroke: A longitudinal fMRI study. Brain 126, 2476–2496. [PubMed: 12937084]

Whishaw IQ, O'Connor WT, and Dunnett SB (1986). The contributions of motor cortex, nigrostriatal dopamine and caudate-putamen to skilled forelimb use in the rat. Brain 109, 805–843. [PubMed: 3779371]

Wong CC, Ramanathan DS, Gulati T, Won SJ, and Ganguly K (2015). An automated behavioral box to assess forelimb function in rats. J. Neurosci. Methods 246, 30–37. [PubMed: 25769277]

Yin HH, Mulcare SP, Hilário MR, Clouse E, Holloway T, Davis MI, Hansson AC, Lovinger DM, and Costa RM (2009). Dynamic reorganization of striatal circuits during the acquisition and consolidation of a skill. Nat. Neurosci. 12, 333–341. [PubMed: 19198605]

Yttri EA, and Dudman JT (2018). A Proposed Circuit Computation in Basal Ganglia: History-Dependent Gain. Mov. Disord. 33, 704–716. [PubMed: 29575303]

Zaaimi B, Edgley SA, Soteropoulos DS, and Baker SN (2012). Changes in descending motor pathway connectivity after corticospinal tract lesion in macaque monkey. Brain 135, 2277–2289. [PubMed: 22581799]

Highlights

- DLS is partially disrupted but still involved in skilled reaching after M1 stroke
- PLC and DLS neural dynamics become more consistent and reliable after rehabilitation
- PLC and DLS reorganize simultaneously during rehabilitation
- Fine-timescale coordination between PLC and DLS activity increases with recovery

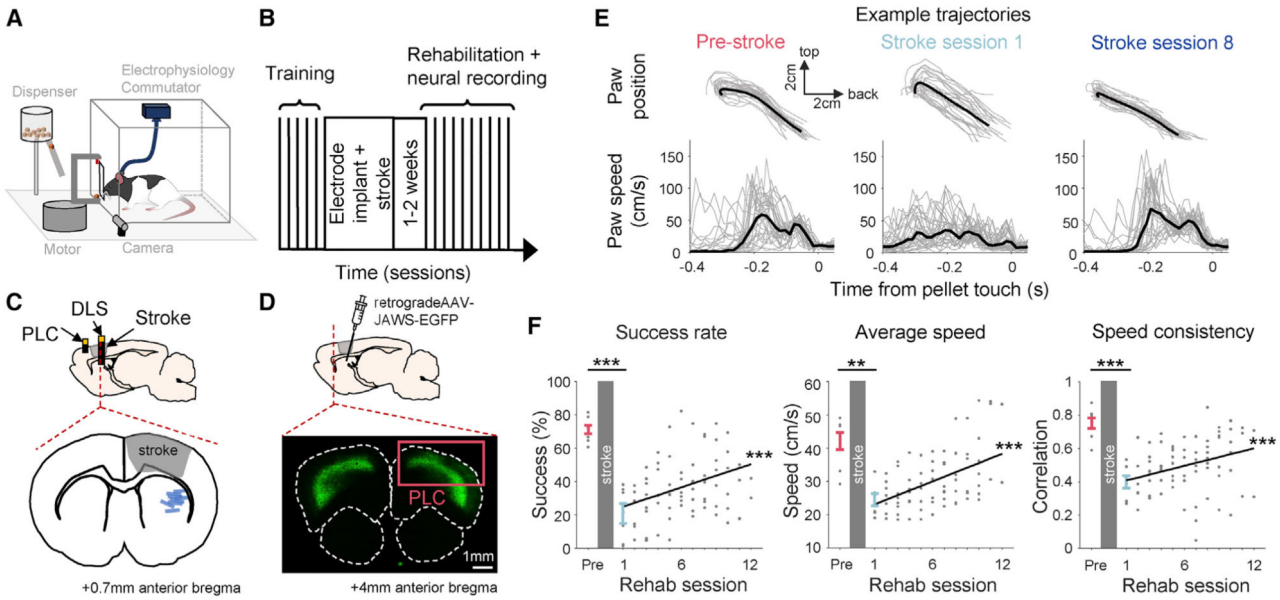

Figure 1. Corticostriatal neural activity was monitored during motor recovery after stroke

(A) Setup for the reach-to-grasp task. The "C" arm rotates to get pellets from the dispenser.

(B) Behavioral paradigm.

(C) Top: sagittal section showing stroke and electrode locations. Bottom: coronal section showing stroke and DLS electrode locations for the eight stroke rats used for electrophysiology recordings. PLC, perilesional cortex; DLS, dorsolateral striatum.

(D) Top: diagram of retrograde tracing from DLS to PLC in stroke rat. Bottom: fluorescent imaging of a coronal section showing projections from PLC to DLS. Green shows GFP-labeled cells.

(E) Paw position (top) and speed (bottom) trajectories for an example rat.

(F) From left to right: pellet retrieval success rate, average speed from reach to pellet touch, and single-trial speed trajectory correlation with pre-stroke mean trajectory over rehabilitation sessions. Each point represents one session from one rat. Error bars represent SEM. The black line is the best-fit line. Asterisks indicate a significant difference between pre-stroke and post-stroke session one using paired t test and significant improvement over rehabilitation sessions using a linear mixed-effects model. $^{**}p < 0.01$, $^{***}p < 0.001$.

See also Figures S1 and S2.

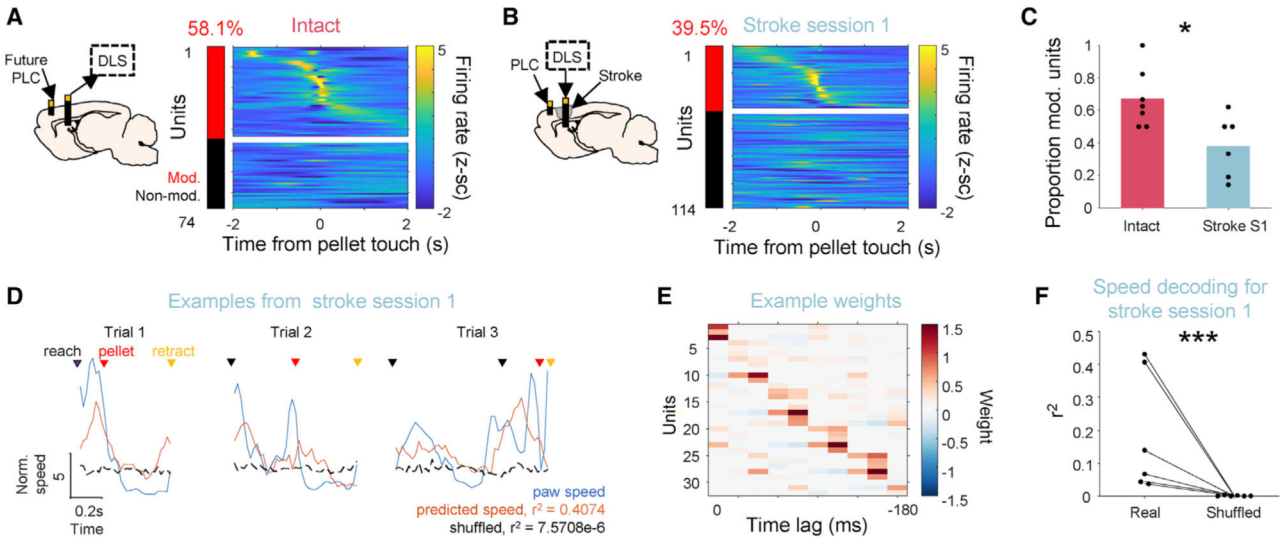

Figure 2. DLS was partially disrupted but still involved in reaching during the first session after stroke

(A and B) Electrode locations (left) and peri-event time histograms (PETHs; right) for all DLS units from seven intact rats and eight stroke rats during the first rehabilitation session, respectively.

(C) Proportion of significantly modulated DLS units in healthy rats versus stroke session 1. Each dot represents one rat, and the bar indicates mean across rats. *$p < 0.05$, using two-sample t test.

(D) Example trials from the first rehabilitation session of a stroke rat showing the actual paw speed, predicted paw speed from DLS unit activity, and predicted speed from shuffled activity.

(E) Weights for multiple linear regression for one example stroke rat.

(F) R^2 values of speed prediction using DLS unit activity versus shuffled activity for the first rehabilitation session post-stroke. Each line represents one rat. ***$p < 0.001$, t test between real and shuffled distributions for each rat.

See also Figure S3.

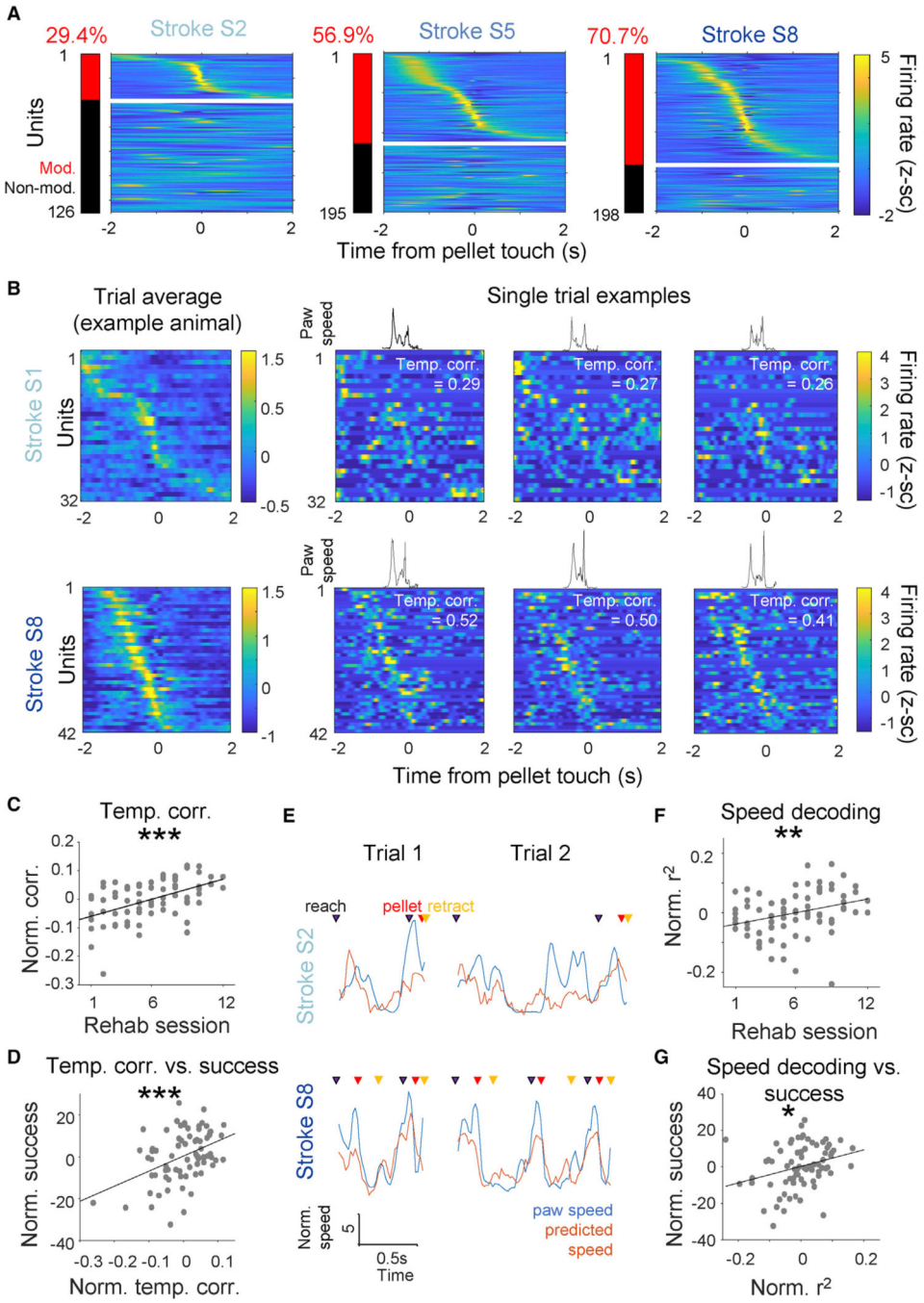

Figure 3. DLS neural dynamics reorganized during rehabilitation

(A) PETH for all DLS units from eight rats during rehabilitation sessions 2, 5, and 8.

(B) Left: average PETH for an example rat. Right: single-trial PETH examples. Black lines on top show paw speed for the single trials.

(C) Single-trial neural correlation with the session template across rehabilitation sessions. Each dot represents the normalized correlation for one session of one rat. The correlation values for each rat were normalized by mean subtraction across sessions of that rat. The black line is the best-fit line based on a linear mixed-effects model.

(D) Correlation between normalized success rate and normalized template correlation. Success rate was normalized by mean subtraction across sessions of each individual rat. Template correlation was normalized as in (C). Same labeling conventions as in (C).
(E) Example paw speed and predicted speed using DLS neural activity for an example rat.
(F) Speed decoding r^2 across rehabilitation. Each dot represents the normalized r^2 for one session of one rat. The r^2 values for each rat were normalized by mean subtraction across sessions of that rat. The black line is the best-fit line.
(G) Correlation between normalized success rate and normalized speed decoding r^2. Success rate was normalized by mean subtraction across sessions of each individual rat. Speed decoding r^2 was normalized as in (F). Same labeling conventions as in (F). $^{**}p < 0.01$, $^{***}p < 0.001$. p values are for the regression coefficient, obtained using a linear mixed-effects model, with session, template correlation, or speeding decoding r^2 as the fixed effect and rat identity as the random effect.
See also Figure S4.

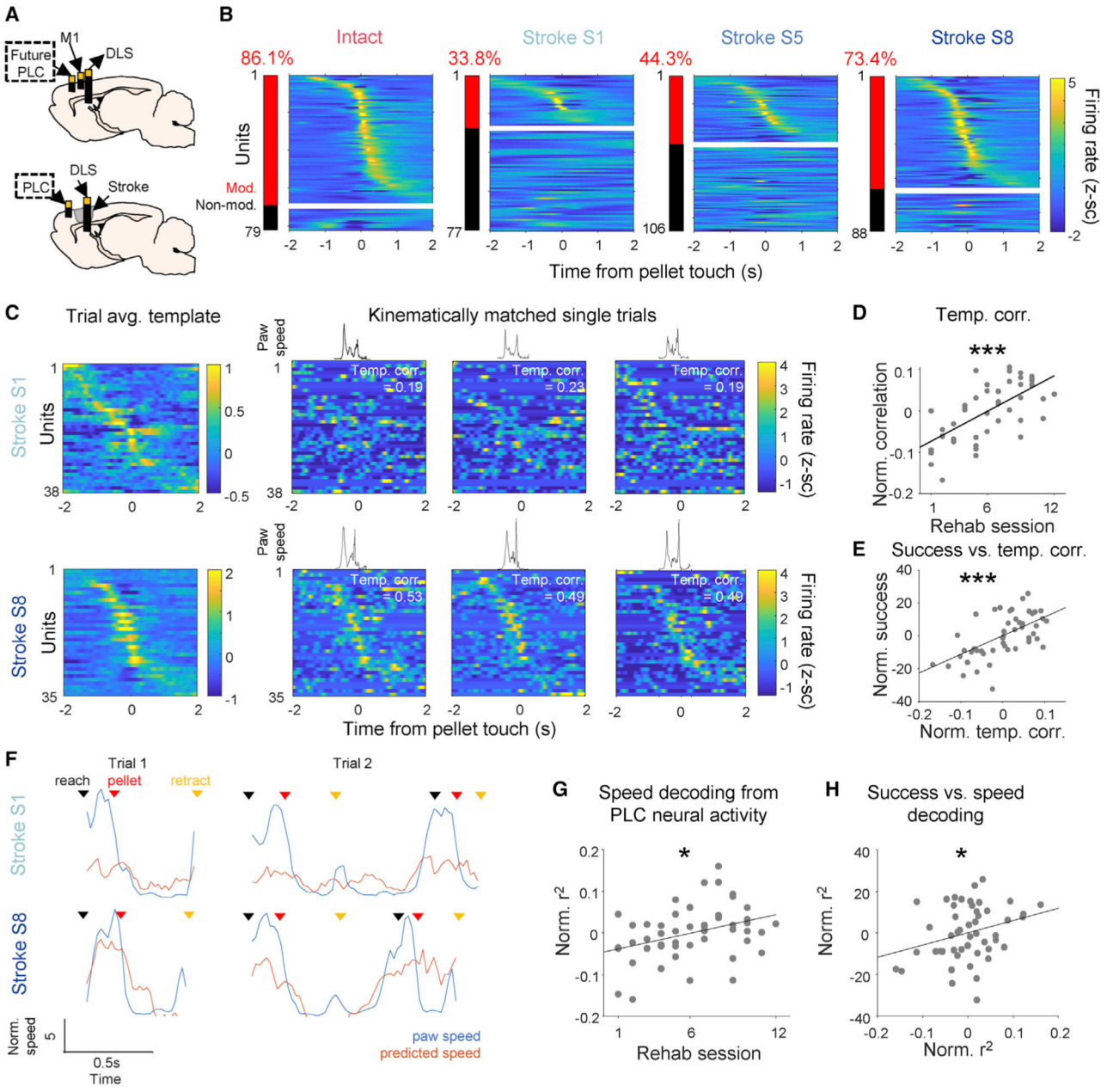

Figure 4. Changes in PLC activity paralleled changes in DLS

(A) Electrode locations for intact and stroke rats.

(B) PETH of all PLC units from healthy rats (n = 3) and sessions 1, 5, and 8 of stroke rats (n = 6).

(C) Left: trial-averaged PETH for all units in an example rat. Right: single-trial PETH examples.

(D) Template correlation across rehabilitation sessions. Each dot represents the normalized correlation for one session of one rat. The correlation values for each rat were normalized by mean subtraction across sessions of that rat. The black line is the best-fit line.

(E) Correlation between normalized success rate and normalized template correlation. Success rate was normalized by mean subtraction across sessions of each rat. Template correlation was normalized as in (D). Same labeling conventions as in (D).
(F) Examples trials from a rat showing actual paw speed and predicted speed using PLC neural activity.
(G) R^2 of speed decoding using PLC activity over rehabilitation. Each dot represents the normalized r^2 for one session of one rat. The r^2 values for each rat were normalized by mean subtraction across sessions of that rat. The black line is the best-fit line.
(H) Correlation between normalized success rate and normalized speeding decoding r^2. Success rate was normalized by mean subtraction across sessions of each individual rat. Speeding decoding r^2 was normalized as in (G). Same labeling conventions as in (G). *$p < 0.05$, ***$p < 0.001$. p values are for the regression coefficient, obtained using a linear mixed-effects model, with session, template correlation, or speeding decoding r^2 as the fixed effect and rat identity as the random effect.
See also Figure S4.

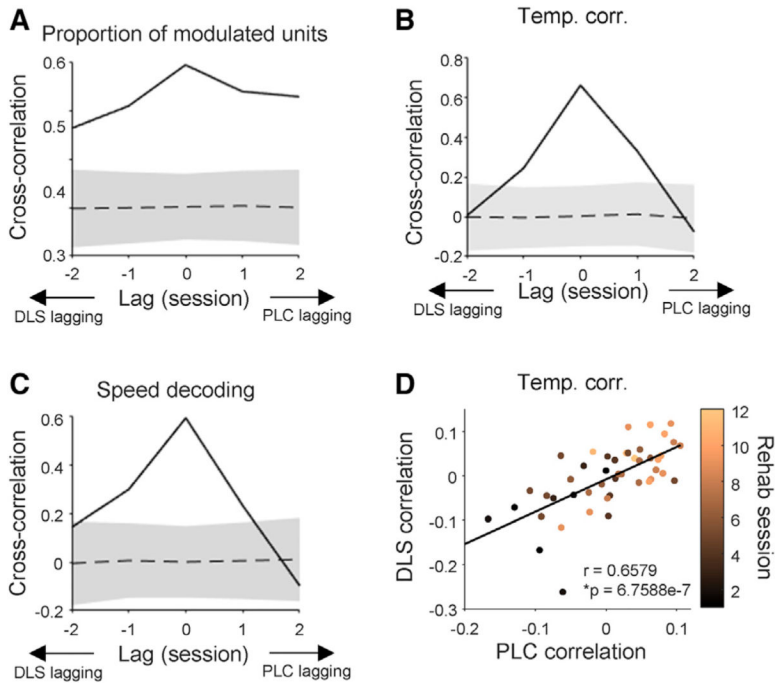

Figure 5. Neural changes in PLC and DLS occurred simultaneously across rehabilitation sessions

(A) Solid black line shows cross-correlation between the proportion of modulated units in PLC and DLS at different time lags. Dotted black line shows the mean and gray shaded area indicates the standard deviation of shuffled distribution.

(B) Cross-correlation of template correlation between PLC and DLS at different time lags. Same labeling conventions as (A).

(C) Cross-correlation between speed decoding r^2 of PLC and DLS at different time lags. Same labeling conventions as (A).

(D) Correlation between template correlation of PLC and DLS across animals and sessions at zero time lag. Each dot represents the normalized template correlation for one session of a rat, colored by rehabilitation session. The black line is the best-fit line.

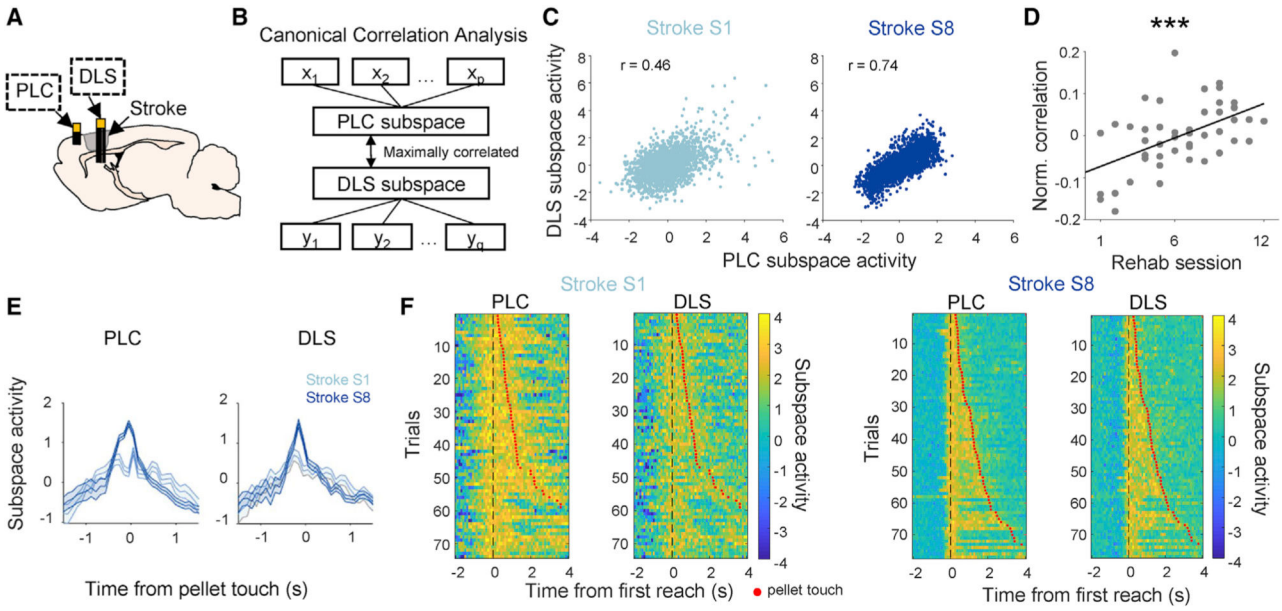

Figure 6. Fine-timescale coordination between PLC and DLS increased after rehabilitation

(A) Simultaneous electrophysiology recording from PLC and DLS.

(B) Description of canonical correlation analysis (CCA). CCA finds a linear combination of binned spike counts from PLC units (x_1, x_2, … x_p) and DLS units (y_1, y_2, …, y_q) that maximizes the correlation between PLC and DLS.

(C) DLS versus PLC subspace activity (from the first canonical component) during movement (−1.5 to 1.5 s around pellet touch) for example sessions from a rat. Each dot represents one time bin of a trial from the session.

(D) PLC-DLS canonical correlation of top component during movement across rehabilitation. Each dot represents the normalized correlation for one session of one rat. The correlation values for each rat were normalized by mean subtraction across sessions of that rat. The black line is the best-fit line. ***$p < 0.001$. p values are for the regression coefficient for rehabilitation session, obtained using a linear mixed-effects model, with session as fixed effect and rat identity as random effect.

(E) PLC and DLS subspace activity against movement time across all trials for an example rat. Solid lines represent the mean, and the shaded area denotes SEM.

(F) PLC and DLS subspace activity from single trials sorted by first reach to pellet touch duration.

See also Figures S5 and S6.

KEY RESOURCES TABLE

REAGENT or RESOURCE	SOURCE	IDENTIFIER
Antibodies		
Mouse anti-NeuN	Millipore	Cat#MAB377; RRID: AB_2298772
Biotinylated anti-mouse IgG secondary antibody	Vector Lab	Cat#BA-9200; RRID: AB_2336171
Bacterial and virus strains		
retrogradeAAV-hSyn-JAWs-KGC-GFP-ER2	Tervo et al., 2016	Addgene; 65014-AAVrg
Chemicals, peptides, and recombinant proteins		
Rose Bengal	Sigma-Aldrich	Cat#330000
Muscimol	Tocris Bioscience	Cat#0289
Fluorescent muscimol. BODIPY TMR-X Conjugate	Invitrogen	Cat#M23400
Vectashield antifade mopunting medium with DAPI	Vector Lab	Cat#H-1200–10
Permount mounting medium	Fisher Scientific	Cat#SP15–100
Critical commercial assays		
ABC kit	Vector Lab	Cat#PK-4000
DAB substrate kit	Vector Lab	Cat#SK-4100
Experimental models: Organisms/strains		
Rat: Long Evans	Charles River Laboratories	CAT#006L/E
Software and algorithms		
MATLAB 2018b	MathWorks	https://www.mathworks.com/products/get-matlab.html?s_tid=gn_getml
ImageJ		https://imagej.nih.gov/ij/
Synapse Suite	Tucker-Davis Technologies	https://www.tdt.com/component/synapse-software/
Offline Sorter V4.3.0	Plexon Inc	https://plexon.com/products/offline-sorter/
Other		
32/64-channel ZIF clip microwire array	Tucker-Davis Technologies	ZIF-32, ZIF-64
4x8 fixed array	Innovative Neurophysiology	N/A
Infusion cannula	PlasticsOne	CAT#C235G, C235I, C235IC
Electrophysiology acquisition system	Tucker-Davis Technologies	RZ2, PZ2, PZ4
Electrical stimulation system	Tucker-Davis Technologies	IZ2
Electrophysiology ZIF clip head stages	Tucker-Davis Technologies	ZC64, ZC32, ZCD32, ZCD64